Stanford Exploration Project, Report 100, April 20, 1999, pages 113–125

Subsalt imaging by common-azimuth migration

Biondo Biondi[1]

keywords: *migration, common-azimuth, wave-equation*

ABSTRACT

The comparison of subsalt images obtained by common-azimuth migration and single-arrival Kirchhoff migration demonstrates the potential of wave-equation migration when the velocity model causes complex multipathing. Subsalt reflectors are better imaged and the typical Kirchhoff artifacts caused by severe multipathing disappear. A detailed analysis of common-azimuth images indicates that the results of common-azimuth imaging could be improved. It points to opportunities to improve the numerical implementation as well as the downward continuation method.

INTRODUCTION

Kirchhoff migration methods often fail to produce satisfactory images of subsalt reflectors because they do not handle correctly multipathing of the reflected energy. When the wavefield is severely distorted by a salt body, or other complex velocity structure, the computation of the multivalued Green functions required by Kirchhoff methods is challenging. Further, even if we were able to compute the Green functions accurately and efficiently, the numerical integration of the wavefield over patchy and multivalued integration surfaces would be a difficult, and probably unreliable, task.

Wave-equation methods are an attractive and robust alternative to the complexities involved in extending Kirchhoff migration to handle correctly multipathing. However, full wave-equation 3-D prestack migration is still too computationally intensive to become a practical tool. Therefore, in the past few years I developed common-azimuth migration that is an approximation to full wave-equation 3-D prestack migration (Biondi and Palacharla, 1996; Biondi, 1997). It exploits the narrow-azimuth nature of marine data to reduce the computational cost by a large factor (20 to 50) with respect to full wave-equation 3-D prestack migration.

I applied common-azimuth migration to the narrow-azimuth subset of SEG-EAGE salt model (Aminzadeh et al., 1996) (known as C3 Narrow-Azimuth classic data set C3-NA (1997)) and compared the results with the results produced by a single-arrival Kirchhoff migration. The data were recorded on the realistic and complex salt-dome structure shown in

[1]**email:** biondo@sep.stanford.edu

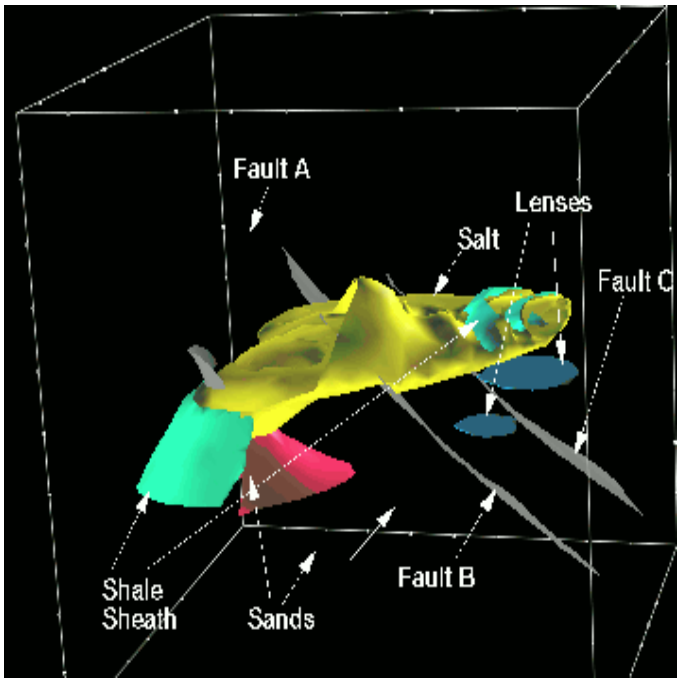

Figure 1: 3-D representation of the SEG-EAGE salt model. biondo1-saltnew-color [NR]

Figure 1. In the subsalt areas, common-azimuth migration resolves the reflectors better than Kirchhoff migration, and yields an image with much less artifacts and spurious reflectors. The run times of common-azimuth migration and Kirchhoff migration were roughly the same. These results confirm the potentiality of wave-equation migration and give new impulse to our efforts to develop a complete wave-equation imaging (migration and velocity analysis) procedure for both structural and stratigraphic imaging.

The lack of a simple and reliable method to extract prestack information from the results of wave-equation migration has been correctly perceived as a serious drawback (Etgen, 1998). It curtailed the usefulness of wave-equation migration for both velocity estimation and Amplitude Versus Angle (AVA) analysis. In Prucha et al. (1999), we show a very simple method to overcome this problem. We slant stack the downward continued wavefield at each depth level and produce high-quality Common Image Gathers (CIG) that display image amplitude as a function of the reflection angle. Sinha and Biondi (1999) discuss an example that compares wave-equation CIGs with the corresponding Kirchhoff CIGs for AVA analysis. Wave-equation CIGs can also be used for estimating migration velocity in a way similar to the common use of Kirchhoff-derived CIGs. Wave-equation CIGs are sensitive to migration velocity errors as the CIG obtained by migrating offset plane waves (Ottolini and Claerbout, 1984; Mosher et al., 1997). However, they are more accurate because they are based on a wavefield decomposition at depth and not at the surface.

Our ultimate goal is to build a complete and self-consistent wave-equation imaging procedure. An indispensable component of wave-equation imaging is a Wave-Equation Migration Velocity Analysis (WEMVA) method. Biondi and Sava (1999) present a WEMVA based on the linearization and inversion of downward continuation operators. WEMVA is more robust and stable than conventional ray-based MVAs because it can easily handle dis-

continuous velocity function and multipathing. The capability of performing both velocity analysis and AVA analysis by wave-equation methods is attractive because it opens the possibility, though still far from being reality, to perform AVA analysis in more complex areas than is possible today. For AVA analysis in complex areas, wave-equation methods have a crucial advantage over asymptotic methods; they can model correctly the amplitudes variations related to the focusing and defocusing of bandlimited wavefields caused by velocity variations.

The results that are presented in this paper also show that Kirchhoff migration produced better images than common-azimuth migration in some areas of the model. At the moment of writing, it is not clear whether the degradation of the common-azimuth migration images was caused by the limitations of the numerical method employed to implement common-azimuth migration, or, by the inherent limitations of the common-azimuth migration method itself. Further investigation is needed. Common-azimuth migration has inherent limitations that are directly related to the approximations needed for its derivation and can be explained by a theoretical analysis (Biondi and Palacharla, 1996). Vaillant and Biondi (1999) discuss a promising method, dubbed narrow-azimuth migration, to overcome these limitations. The new method is more expensive than common-azimuth migration but it is still an order of magnitude cheaper than full wave-equation migration.

SEG/EAGE SALT DATA SET AND PREPROCESSING

The Salt Model C3-NA data set simulates a narrow-azimuth marine acquisition with 8 streamers recorded on an area about one quarter of the whole model. The maximum absolute offset is about 2,600 m and the maximum cross-line offset between the sources and the outer streamers is $\pm$ 140 m. The in-line direction is East-West, corresponding to the approximate North-South direction in the model as displayed in Figure 1. Notice that the figure displays the model rotated with respect to its “true” orientation; that is, the “true North” of the model points to the West of the figure.

The salt body in the model exhibits steep flanks near the crest and a rough surface on the top of the shelf. These characteristics cause severe distortions in the wavefield propagating through the salt. The reflectors below the salt area are thus poorly illuminated by data acquired with narrow-azimuth marine-like geometry. Consequently, the imaging of subsalt reflector is spotty even when using full-wave equation methods (Ober and Oldfield, 1999). Furthermore, deep dipping reflectors cannot be imaged because of the limited spatial extent of the data set. To reduce the computational cost of the modeling effort, the data were acquired on a dense grid only on a subset of the model. Good reference reflectors are: the bottom of the salt, the flat strong reflector at the bottom of the model (not marked in Figure 1), and the two sand lenses marked as "Lenses" in Figure 1. The bottom of the salt can be imaged pretty well in most of the areas, with the exception of the root proximities, where the interfaces are steeply dipping.

Before common-azimuth migration, the narrow-azimuth data were transformed to effective common-azimuth data by applying Azimuth Moveout (Biondi et al., 1998). The

regularized common-azimuth data set was binned with a 20 meters CMP spacing in both the in-line and cross-line directions, and with 100 meters sampling along the in-line offset direction. With 100 meters offset spacing, the moveouts of the shallow events are aliased. However, because the dips along the offset can be safely assumed to be always positive, aliasing by a factor of two can be easily overcome by both wave-equation migration and Kirchhoff migration (Biondi, 1998b). The data were muted with a "deep" mute because the early arrival are contaminated by all sorts of modeling noise. This mute affected the imaging of the shallow events. A more careful mute could accomplish both goals of noise removal and shallow events preservation. Kirchhoff migration is more flexible than common-azimuth migration with respect to the input-data geometry. Therefore, the original narrow-azimuth data were migrated by Kirchhoff migration.

MIGRATION RESULTS

Figure 2 shows a typical in-line section through the velocity model, taken at the constant cross-line coordinate y=6,850 m. Figure 3 shows the corresponding common-azimuth migration results. Almost perfect images are obtained for the reflectors in the sediment above the salt, the top and the bottom of the salt. The flat 'basement' is well imaged in some areas and not in others. The dipping reflectors in the subsalt are not easily distinguishable from the background noise, if they are present at all. The good results above the salt are to be expected from common-azimuth migration. Prestack time migration would have produced similarly good results. However, poststack migration after constant velocity DMO would have had trouble to image correctly the steep faults that terminate at the top of the salt because of NMO-velocity conflicts (Rietveld et al., 1997; Biondi, 1998a).

The focus of this paper is on the subsalt region, and on the comparison with Kirchhoff migration results. Figure 4 shows the in-line section taken through the velocity cube at constant cross-line coordinate y=9,820 m . This section is interesting because it crosses both sand lenses in the subsalt. Further, between the lenses there is an anticlinal structure broken by converging normal faults that has some chances to be visible in the images because it is flattish. Figure 5 shows the subsalt images obtained by Kirchoff migration (top) and common-azimuth migration (bottom). The common-azimuth image is superior to the Kirchhoff image in several ways. First, the common-azimuth image lacks the strong coherent artifacts that makes the Kirchhoff image difficult to interpret. These artifacts are caused by partially coherent stacking of multipathing events along wrong trajectories. They are typical of Kirchhoff subsalt images, and can be only partially removed by a "smart" selection of the Kirchhoff summation surfaces, such as the ones suggested by the most-energetic arrival or shortest-path criteria (Nichols et al., 1998). Second, both lenses are interpretable from the common-azimuth image while in the Kirchhoff image they are either lost in the noise (top lens) or completely missing (bottom lens). Third, both the bottom of the salt and the basement are more continuous in the common-azimuth image. On the other hand, the large fault visible on the left part of the section at (1,800-4,000 m) is not perfectly imaged by common-azimuth migration. I will analyze this problem in more detail at the end of this section with the help of cross-line sections (Figure 9, Figure 10 and Figure 11).

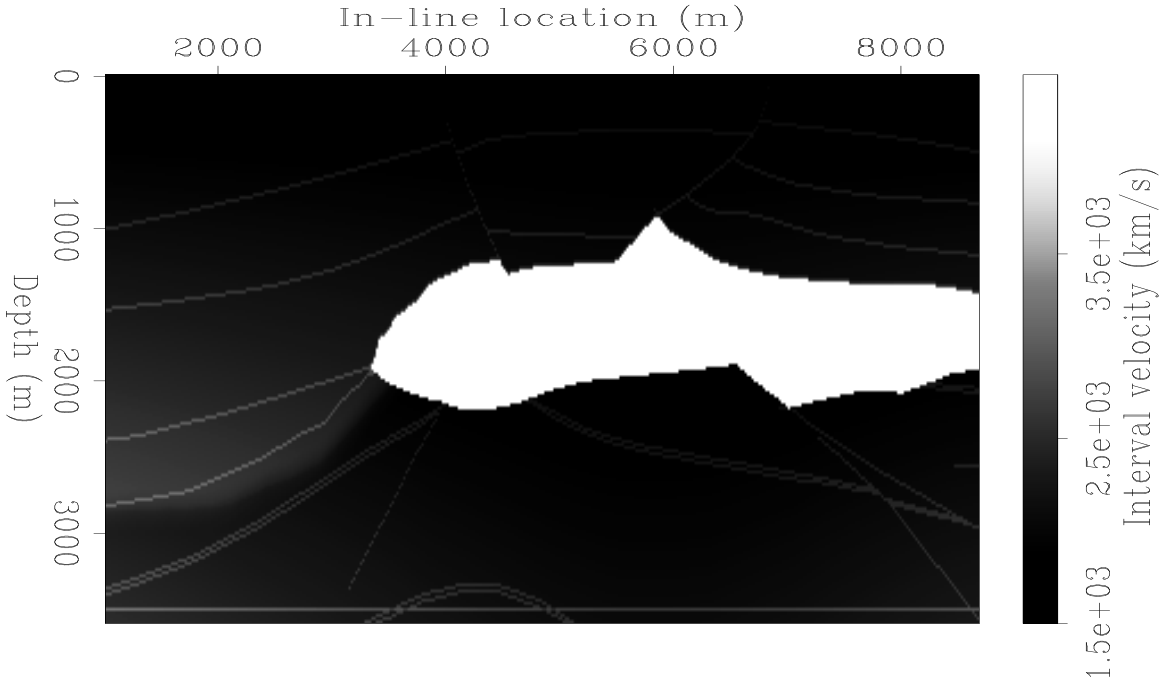

Figure 2: Velocity model at constant cross-line coordinate y=6,850 m. biondo1-Vel-salt-y6850 [CR]

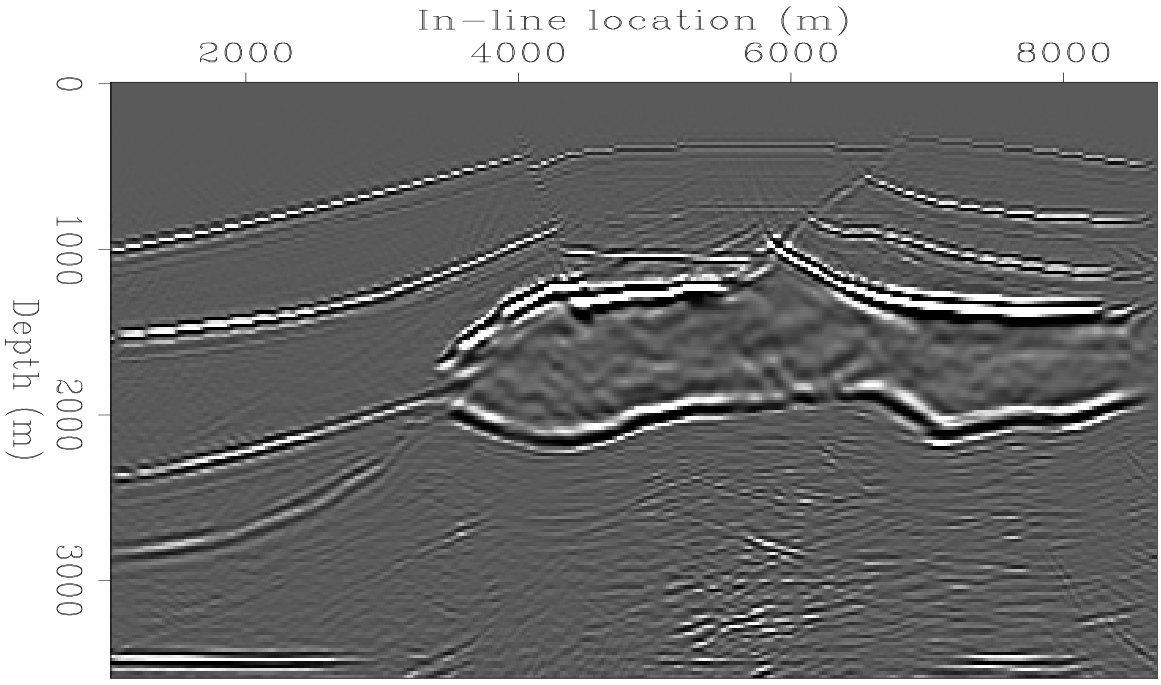

Figure 3: Common-azimuth migration at constant cross-line coordinate y=6,850 m. biondo1-Wave-salt-whole-y6850 [CR]

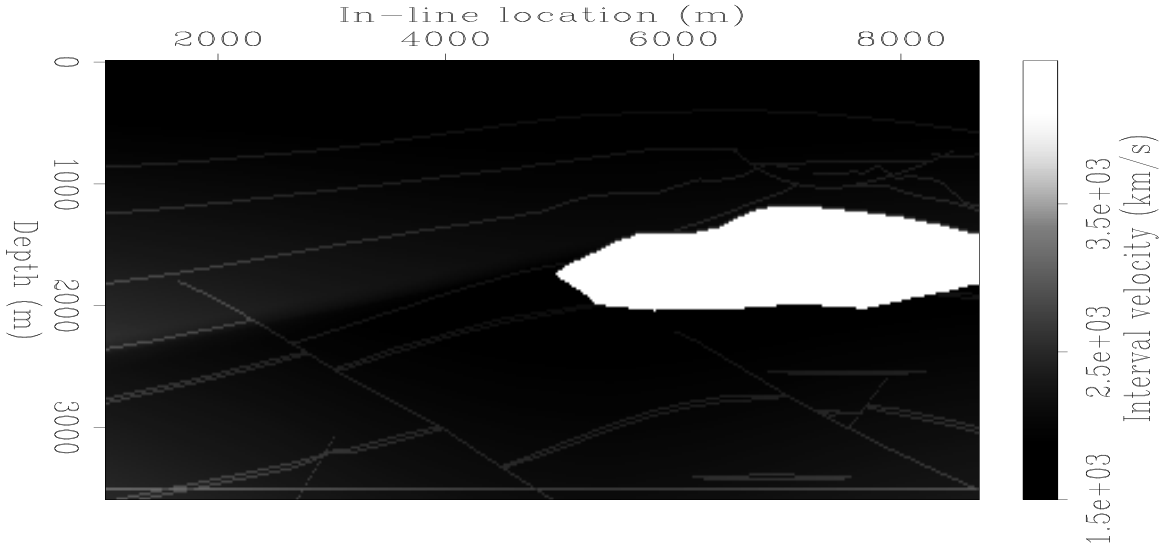

Figure 4: Velocity model at constant cross-line coordinate y=9,820 m. biondo1-Vel-salt-y9820 [CR]

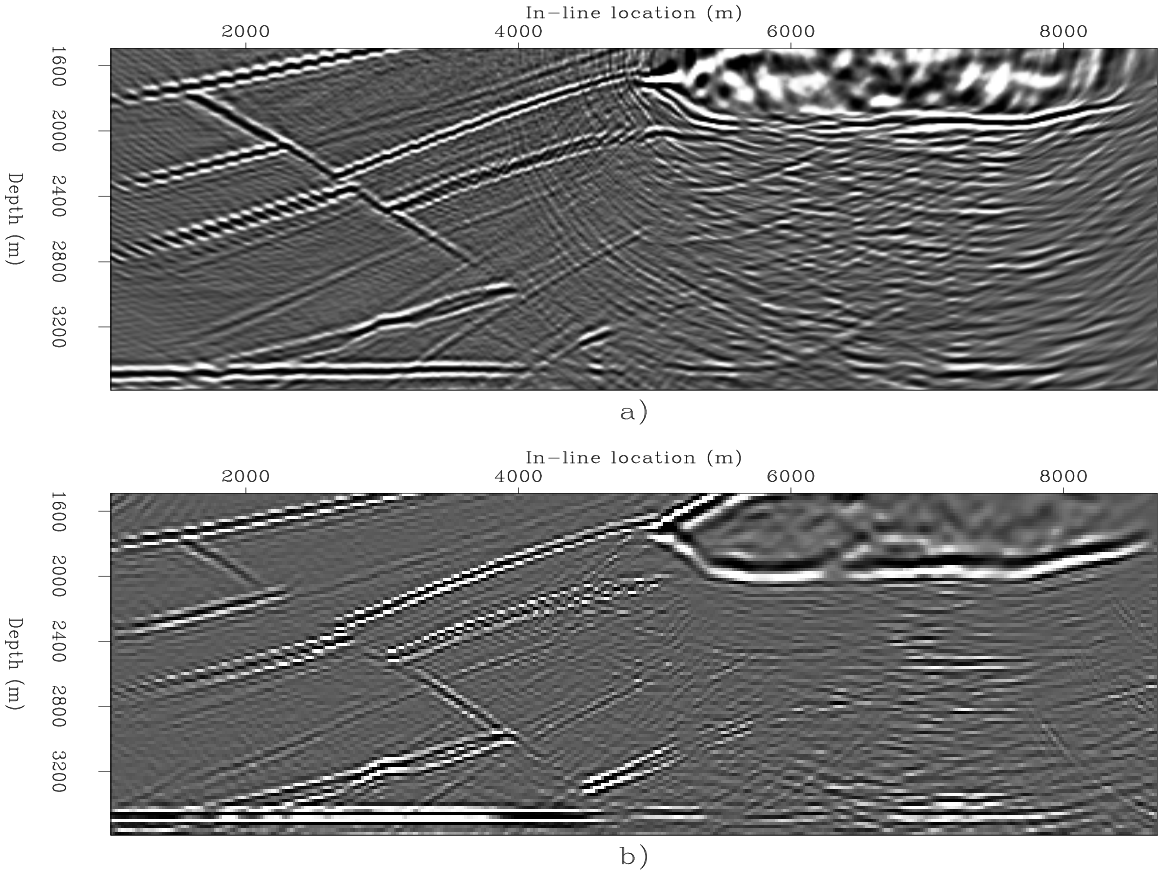

Figure 5: Kirchhoff migration (a) and common-azimuth migration (b) at constant cross-line coordinate y=9,820 m. Both sections are rendered using the same (98) percentile for clipping amplitudes. biondo1-Both-salt-under-y9820 [CR]

Figure 6 shows the cross-line section taken through the velocity cube at constant in-line coordinate y=7,440 m. This cross-line section passes through the two subsalt lenses as the in-line section shown in Figure 4. Figure 7 shows the corresponding migrated images; Kirchhoff migration on the top and common-azimuth migration on the bottom. As before, the two lenses are clearly interpretable in the common-azimuth image, whereas they are not in the Kirchhoff image. However, in this case the central portion of the salt bottom is not perfectly imaged in either of the two images. This area is right below the deep canyons in the salt body visible in Figure 6. The steep flanks of the canyons, and the large velocity contrast between the salt body and the soft sediments filling the canyons, cause a severe distortion of the reflected wavefield. The bottom of the salt and the reflectors below, including the basement, are thus poorly illuminated. In the column below the canyons, the Kirchhoff image shows strong artifacts that could be easily interpreted as reflections. The common-azimuth image is much cleaner, although without interpretable coherent events. The poor reflectors' illumination below the canyons can be analyzed further by looking at the Common Image Gathers (CIG) displayed in Figure 8. The gather on the left corresponds to a cross-line location right below the canyons; the one on the right is further toward the right. In both gathers, the images of the reflectors above the salt and the top-of-salt are well imaged and are aligned nicely along the offset ray parameter axis. In the gather on the right, the bottom of the salt, the shallower lens, the deeper lens, and the basement are also coherent and well aligned horizontally. But in the gather on the left, there is very little coherent energy below the salt.

Finally, I analyze the question of the poor imaging by common-azimuth migration of the fault shown in Figure 5. Figure 9 and Figure 10 show respectively the velocity model and the migrated images at constant in-line coordinate x=2,560 m. The fault under study is the fault on the right part of the sections. The deeper part of the fault is not illuminated by the data because of lack of spatial coverage, and thus is not imaged by either Kirchhoff migration or common-azimuth migration. The shallower part of the fault is well imaged by both migrations, but the middle part of the fault is well imaged by Kirchhoff migration and not by common-azimuth migration. The poor imaging seems to be correlated with the velocity inversion right above the fault visible in the velocity sections (Figure 4 and Figure 9). Both the geological dip and the local gradient of the velocity function are roughly oriented at an angle of 45 degrees with respect to the shooting direction. Therefore, they have a large component in the cross-line direction, creating the conditions under which the approximations inherent in common-azimuth migration are the worst (Biondi and Palacharla, 1996). On the other hand, the problem may be simply caused by the fact that I used too few reference velocities (three) when I downward continued the wavefield with an extended split-step method. This issue deserves more studies and to investigate it further. I am now developing a better common-azimuth continuation method based on Ristow's Fourier finite-difference methodology (Ristow and Ruhl, 1994).

Both Kirchhoff migration and common-azimuth migration have trouble to image the two deeper flattish reflectors at cross-line location of about 7,000 meters. The culprit seems to be again the sharp velocity contrast above the fault. However, the problem may be caused by the salt edge above the reflectors, not visible in these sections.

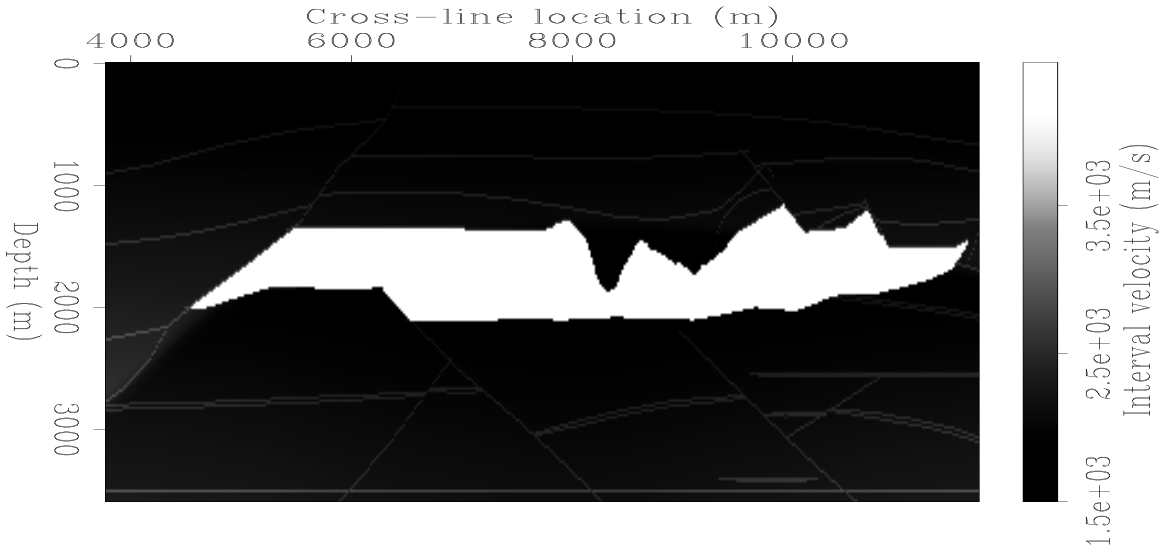

Figure 6: Velocity model at constant in-line coordinate x=7,440 m. biondo1-Vel-salt-x7440 [CR]

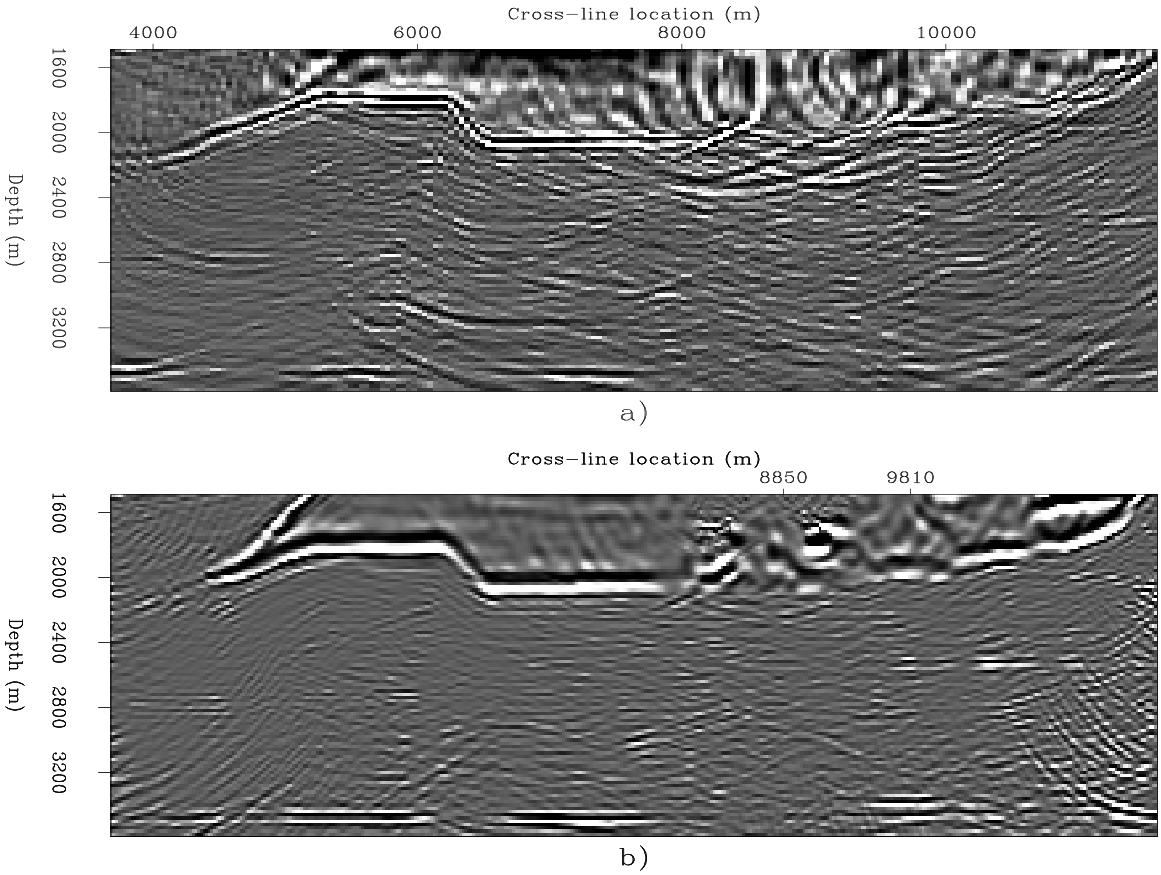

Figure 7: Kirchhoff migration (a) and common-azimuth migration (b) at constant in-line coordinate x=7,440 m. Both sections are rendered using the same (98) percentile for clipping amplitudes. biondo1-Both-salt-under-x7440 [CR]

Figure 11 shows the CIG gathers taken at both problematic locations. The gather on the left shows some coherent energy for the poorly imaged reflections, though the energy is not perfectly aligned along the ray-parameter axis. The gather on the right shows no coherent energy corresponding to the poorly imaged fault, suggesting a worse imaging problem for this case.

CONCLUSIONS

Common-azimuth migration produced better results in the subsalt than a single-arrival Kirchhoff migration. The subsalt reflectors are much more interpretable in the common-azimuth images than in the Kirchhoff images, both because the images are devoid of the typical subsalt Kirchhoff artifacts and because the reflectors themselves are better imaged.

Although superior to Kirchhoff images, the common-azimuth images in the subsalt are far from perfect. Sub-optimal images are probably caused by a combination of poor reflectors' illumination and inaccuracies in the migration procedure. The shortcomings in the migration procedure are of two types: common-azimuth approximations and numerical approximations. We plan to address both types. We are developing a narrow-azimuth extension to common-azimuth migration (Vaillant and Biondi, 1999). And we plan to apply to common-azimuth downward continuation more accurate numerical methods that are based on a combination of the helix (Rickett et al., 1998) and Ristow's Fourier finite-difference methods (Ristow and Ruhl, 1994).

REFERENCES

Aminzadeh, F., Burkhard, N., Long, J., Kunz, T., and Duclos, P., 1996, Three dimensional SEG/EAGE models - an update: The Leading Edge, **2**, 131–134.

Biondi, B., and Palacharla, G., 1996, 3-D prestack migration of common-azimuth data: Geophysics, **61**, 1822–1832.

Biondi, B., and Sava, P., 1999, Wave-equation migration velocity analysis: SEP–**100**, 11–34.

Biondi, B., Fomel, S., and Chemingui, N., 1998, Azimuth moveout for 3-D prestack imaging: Geophysics, **63**, no. 2, 574–588.

Biondi, B., 1997, Azimuth moveout + common-azimuth migration: Cost-effective prestack depth imaging of marine data: 67th Annual Internat. Mtg., Soc. Expl. Geophys., Expanded Abstracts, 1375–1378.

Biondi, B., 1998a, Azimuth moveout vs. dip moveout in inhomogeneous media: 68th Ann. Internat. Meeting, Soc. Expl. Geophys., 1740–1743.

Biondi, B., 1998b, Kirchhoff imaging beyond aliasing: submitted for publication to Geophysics.

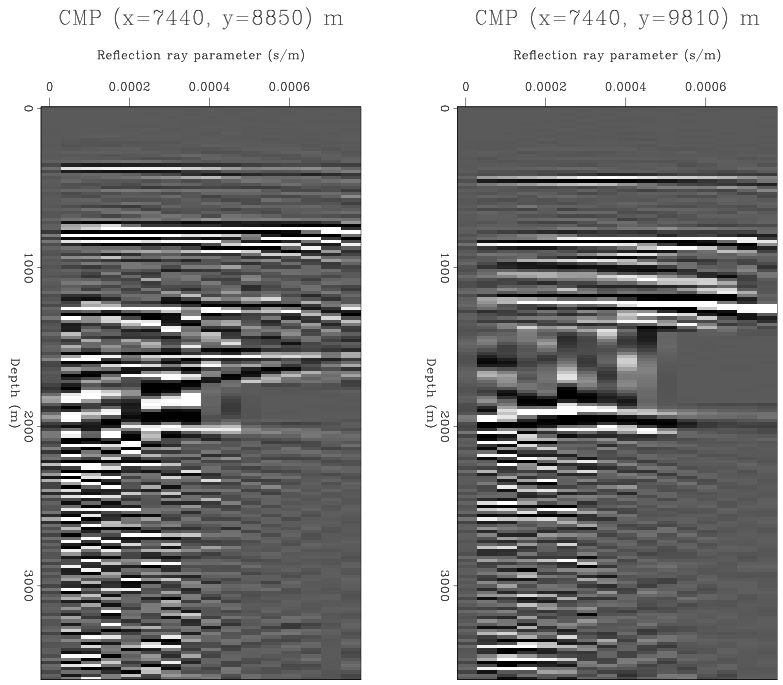

Figure 8: Angle-domain Common Image Gathers obtained by common-azimuth migration. The locations of these CIGs are marked on the in-line axis of the common-azimuth image shown in Figure 7 biondo1-AVO-salt-8850-9810-x7440 [CR]

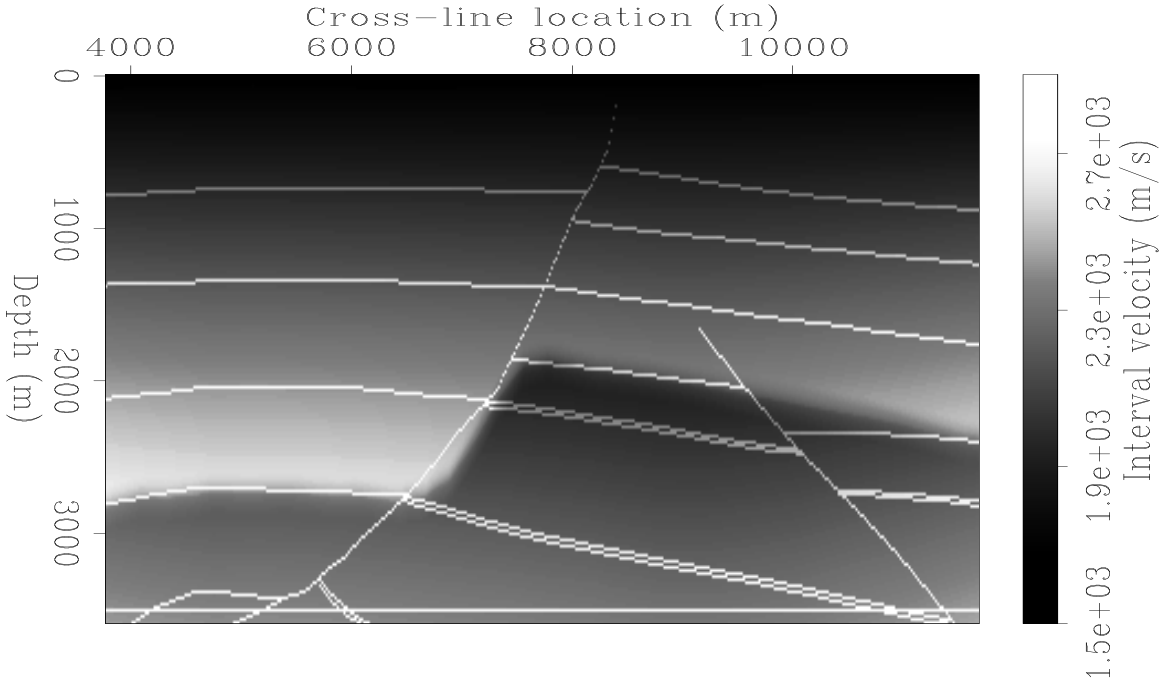

Figure 9: Velocity model at constant in-line coordinate x=2,560 m. biondo1-Vel-salt-x2560 [CR]

Etgen, J. T., 1998, V(z) F-K prestack migration of common-offset common-azimuth data volumes, part I: theory: 68th Annual Internat. Mtg., Soc. Expl. Geophys., Expanded Abstracts, 1835–1838.

Mosher, C. C., Foster, D. J., and Hassanzadeh, S., 1997, Common angle imaging with offset plane waves: 67th Annual Internat. Mtg., Soc. Expl. Geophys., Expanded Abstracts, 1379–1382.

Nichols, D. E., Farmer, P., and Palacharla, G., 1998, Improving prestack imaging by using a new ray selection method: 68th Annual Internat. Mtg., Soc. Expl. Geophys., Expanded Abstracts, 1546–1549.

Ober, C., and Oldfield, R., 1999, 3D Seismic Imaging of Complex Geologies: http://www.cs.sandia.gov/ ccober/seismic/Salvo.html.

Ottolini, R., and Claerbout, J. F., 1984, The migration of common-midpoint slant stacks: Geophysics, **49**, no. 03, 237–249.

Prucha, M. L., Biondi, B. L., and Symes, W. W., 1999, Angle-domain common image gathers by wave-equation migration: SEP–**100**, 101–112.

Rickett, J., Claerbout, J., and Fomel, S., 1998, Implicit 3-D depth migration by wavefield extrapolation with helical boundary conditions: 68th Ann. Internat. Meeting, Soc. Expl. Geophys., 1124–1127.

Rietveld, W. E. A., Marfurt, K. J., and Kommedal, J. H., 1997, The effect of 3-D prestack seismic migration on seismic attribute analysis: 67th Annual Internat. Mtg., Soc. Expl. Geophys., Expanded Abstracts, 1367–1370.

Ristow, D., and Ruhl, T., 1994, Fourier finite-difference migration: Geophysics, **59**, no. 12, 1882–1893.

SEG-EAGE, 1997, Salt Model Narrow-Azimuth Classic dataset (C3-NA): http://archive.llnl.gov/SSD/classic/classicSalt.html#salt-c.

Sinha, M., and Biondi, B., 1999, Comparing Kirchoff with wave equation migration on a hydrate region: SEP–**100**, 135–140.

Vaillant, L., and Biondi, B., 1999, Extending common-azimuth migration: SEP–**100**, 125–134.

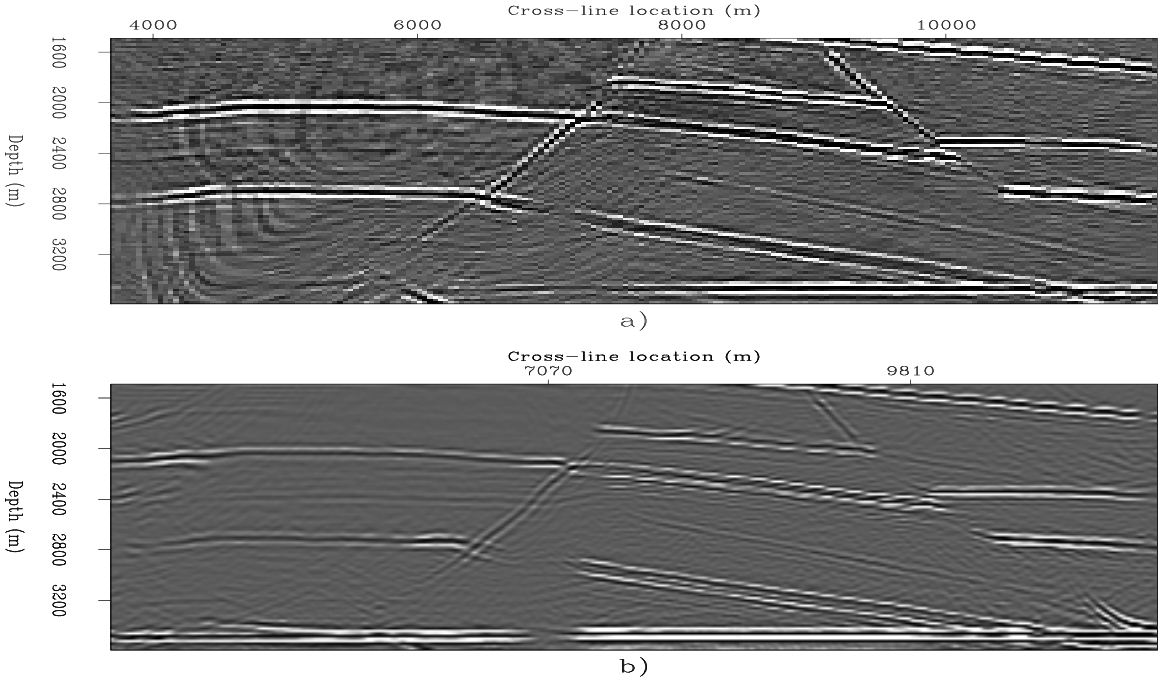

Figure 10: Kirchhoff migration (a) and common-azimuth migration (b) at constant in-line coordinate x=2,560 m. Both sections are rendered using the same (98) percentile for clipping amplitudes. biondo1-Both-salt-under-x2560 [CR]

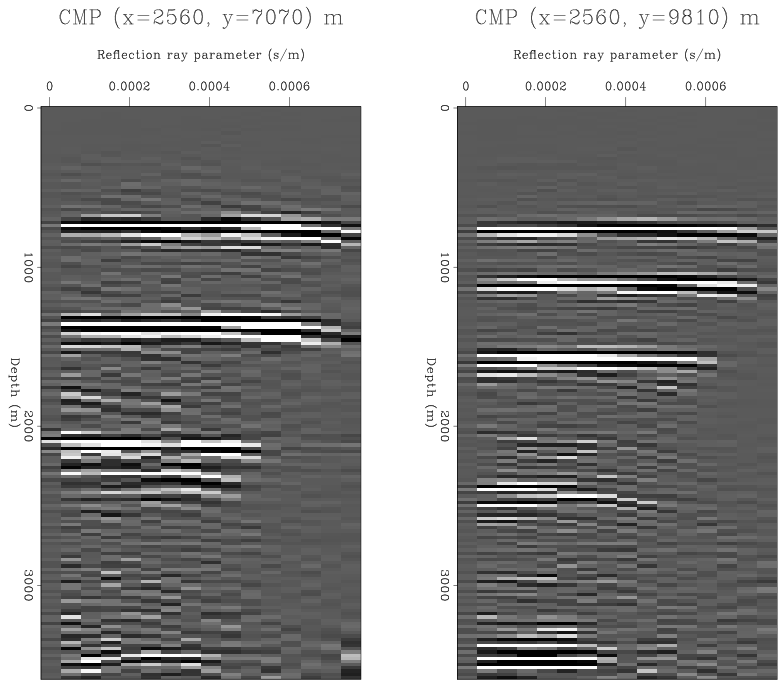

Figure 11: Angle-domain Common Image Gathers obtained by common-azimuth migration. The location of these CIGs are marked on the in-line axis of the common-azimuth image shown in Figure 10 biondo1-AVO-salt-7070-9810-x2560 [CR]